Hindawi
Wireless Communications and Mobile Computing
Volume 2020, Article ID 5791436, 10 pages
https://doi.org/10.1155/2020/5791436

Research Article

Nonorthogonal Multiple Access for Visible Light Communication IoT Networks

Chun Du,[1] Shuai Ma,[1] Yang He,[1] Songtao Lu,[2] Hang Li,[3] Han Zhang,[4] and Shiyin Li[1]

[1] *School of Information and Control Engineering, China University of Mining and Technology, Xuzhou 221116, China*
[2] *IBM Research AI, IBM Thomas J. Watson Research Center, Yorktown Heights, New York 10598, USA*
[3] *Shenzhen Research Institute of Big Data, Shenzhen 518172, China*
[4] *Department of Electrical and Computer Engineering, University of California, Davis, CA 95616, USA*

Correspondence should be addressed to Shuai Ma; mashuai001@cumt.edu.cn

Received 7 January 2020; Revised 7 February 2020; Accepted 17 February 2020; Published 5 May 2020

Guest Editor: Di Zhang

In this study, we investigated the nonorthogonal multiple access (NOMA) for visible light communication (VLC) Internet of Things (IoT) networks and provided a promising system design for 5G and beyond 5G applications. Specifically, we studied the capacity region of a practical uplink NOMA for multiple IoT devices with discrete and continuous inputs, respectively. For discrete inputs, we proposed an entropy approximation method to approach the channel capacity and obtain the discrete inner and outer bounds. For the continuous inputs, we derived the inner and outer bounds in closed forms. Based on these results, we further investigated the optimal receiver beamforming design for the multiple access channel (MAC) of VLC IoT networks to maximize the minimum uplink rate under receiver power constraints. By exploiting the structure of the achievable rate expressions, we showed that the optimal beamformers are the generalized eigenvectors corresponding to the largest generalized eigenvalues. Numerical results show the tightness of the proposed capacity regions and the superiority of the proposed beamformers for VLC IoT networks.

1. Introduction

As the wireless data traffic exponentially increased in 5G, traditional radio frequency- (RF-) based Internet of Things (IoT) network suffers from a limited data rate and network capacity due to the shortage of RF spectra and massive IoT devices. With its vast unlicensed bandwidth, visible light communication (VLC) is a promising complementary solution to meet the growing wireless traffic demands for IoT networks [1, 2]. By exploiting the widespread deployment of the light-emitting diodes (LEDs) as transmitters, VLC has attracted an increasing interest due to its dual functionality: communication and illumination [3–5]. Besides a wider spectrum, VLC has other inherent advantages such as high spatial reuse, high energy efficiency, no electromagnetic radiation, and inherent security [6, 7].

Thus far, traditional IoT networks have generally utilized orthogonal multiple access (OMA) techniques such as frequency division multiple access (FDMA) and time division multiple access (TDMA). In OMA, the resources are allocated orthogonally to multiple users, and it cannot provide sufficient resource reuse. In contrast, the nonorthogonal multiple access (NOMA) technique exploits the power domain for multiple access and is able to serve multiple users at the same time frequency-code resource [8–10], which has recently been included into the 3GPP long-term evolution advanced standard [11–13] and is widely recognized as a promising candidate for the MAC scheme in 5G-enabled IoT applications.

Recently, uplink NOMA has received significant research attention [14–20]. Based on the theory of the Poisson cluster process, the authors in [14] have provided a framework to analyze the rate coverage probability. In [15], the optimal user pairing was investigated for various uplink NOMA scenarios. In [16], the joint subchannel assignment and power allocation problem were investigated. In [17], an interference balance power control scheme was derived. By using stochastic geometry, a signal alignment-based framework was developed in [18] for both multiple-input, multiple-output- (MIMO-) NOMA downlink and uplink transmissions. In [19], a theoretical framework was proposed to analyze the outage probability and the average achievable rate in NOMA downlink and uplink multicell wireless systems. In [20], a phase predistorted joint detection method was proposed to reduce the bit error ratio (BER) for uplink NOMA in VLC systems. Most of the aforementioned research works focused on the RF uplink NOMA [14–19], while the VLC uplink NOMA is not well discussed [20]. Until now, the achievable rate expression of VLC uplink NOMA is still unknown, which makes it great difficult to undertake the optimal NOMA beamforming design for VLC IoT networks.

Different from the RF communications, VLC generally adopts intensity modulation and direct detection (IM/DD), where the messages are modulated to the intensity of the signals. Therefore, the transmitted VLC signals are real and nonnegative, which differ from the RF complex-valued signals. Additionally, due to the eye safety standards and physical limitations, both the peak and average amplitudes of VLC signals are restricted. Hence, the classic Shannon capacity formula with Gaussian input [21] cannot quantify the capacity of VLC IoT networks.

This study is aimed at providing a solution to the above-mentioned issues in the area of VLC IoT networks. First, we investigated the capacity region of MAC in VLC IoT networks. Then, we further studied the optimal beamforming design in a practical NOMA uplink. The main contributions of this study are summarized as follows:

(i) Due to the peak optical power constraint, the optimal input is discrete [22]. Thus, we supposed that the input follows a discrete distribution and develops both the inner and outer bounds of the capacity region of uplink NOMA in VLC IoT networks. Specifically, finding the capacity region was formulated as an entropy maximization problem which is a mixed discrete optimization problem. To overcome the challenge, we proposed an entropy maximization approximation method and obtained the capacity bounds

(ii) Based on the continuous inputs, a closed-form expression for the achievable rate of uplink NOMA of VLC IoT networks is presented. Specifically, with the continuous inputs, the channel capacity of uplink NOMA in VLC IoT networks can be approximated as a differential entropy maximization problem. The corresponding optimal continuous distributions were ABG distributions, and we obtained both the inner and outer bounds in closed forms. To the best of our knowledge, the proposed inner and outer bounds are the first theoretical bounds of the channel capacity region for uplink NOMA of VLC IoT networks

(iii) Finally, based on the obtained results of NOMA, we further studied the optimal receiver beamforming design for VLC IoT. Specifically, we first extended the ABG inner bound to a single-input, multiple-output (SIMO) uplink NOMA case and then maximized the minimum uplink rate of multiple users under receiver power constraints. By exploiting the structure of the achievable rate expression, we equivalently reformulated this problem as a generalized eigenvalue maximization problem, and the optimal beamformers are the generalized eigenvectors corresponding to the largest generalized eigenvalues

The rest of this paper is organized as follows. In Section 2, the capacity regions of the discrete and continuous distribution for uplink NOMA of VLC IoT networks are presented. In Section 3, the achievable rate of multi-LED and optimal beamforming design derived for uplink NOMA of VLC IoT networks is described. In Section 4, the simulation results of the capacity regions and optimal beamforming design in NOMA VLC IoT networks are presented. Finally, the conclusions are presented in Section 5.

2. Capacity Region of Uplink NOMA for VLC IOT Networks

As shown in Figure 1, N single-LED users (IoT devices) simultaneously transmit its own information to a single-PD base station (BS) over the same channel. Let s_i be the message of the ith user, where $|s_i| \le A_i$, $\mathbb{E}\{s_i\} = 0$, and $\mathbb{E}\{s_i^2\} = \varepsilon_i$.

The transmitted signal of the ith user is given by

$$x_i = \sqrt{p_i} s_i + b_i, \tag{1}$$

where p_i is the transmit power of the ith user and b_i is the direct current (DC) bias of the ith user. To ensure that the transmitted signal is nonnegative, the DC bias needs to satisfy $b_i \ge \sqrt{p_i} A_i$.

As the received signal power is dominated by the power from the line-of-sight (LOS) link [23, 24], the diffuse link can be neglected. Thus, the channel gain between user i and the BS is given by [25]

$$g_i = \begin{cases} \dfrac{(m+1)A_R}{2\pi d_\kappa^2} \cos^m(\phi_k) \cos(\psi_k), & \text{if } |\psi_k| \le \psi_{\text{FOV}}; \\ 0, & \text{otherwise}, \end{cases} \tag{2}$$

where m is the Lambertian index of the LED, which depends on the semiangle $\phi_{1/2}$ by $m = -\log 2/(\log(\cos(\phi_{1/2})))$; d_i denotes the distance between user i and the receiver; ϕ is the angle of irradiance; ψ_i is the angle of incidence; ψ_{FOV} is the field of vision (FOV) semiangle of the receiver; and A_R denotes the effective area of the PD.

The received signal at the BS is given by

$$y = \sum_{i=1}^{N} g_i(\sqrt{p_i} s_i + b_i) + z, \tag{3}$$

where $z \sim \mathcal{N}(0, \sigma^2)$ represents the sum of contributions from the shot noise and the thermal noise [26, 27]. At the BS, the

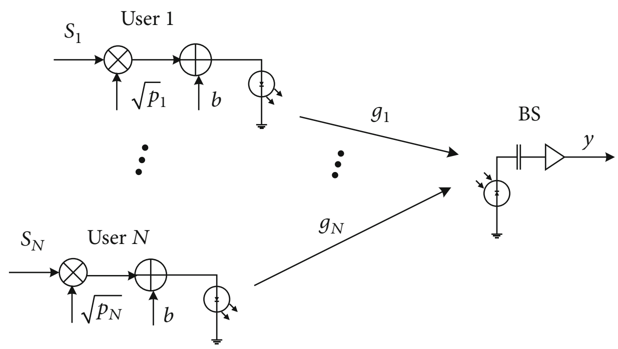

Figure 1: Schematic of an uplink NOMA of VLC IoT network.

multiple received signals may cause interference to each other. To mitigate the interference, the BS applies SIC to decode and remove the partial interference. Without the loss of generality, we assume that the terms $\{g_i^2 \varepsilon_i\}_{i=1}^N$ satisfy a descending order, i.e., $g_1^2\varepsilon_1 \geq g_2^2\varepsilon_2 \geq \cdots \geq g_N^2\varepsilon_N$. The BS adopts the SIC technique to decode the received signals in a descending order [28–31], i.e., from s_1 to s_N. Specifically, when the BS decodes s_i, it first decodes the signal intended for user s_k with the order $k \leq i$ and then subtracts it from y.

Thus far, the capacity region of uplink NOMA for VLC IoT networks has been an open problem, which is a major barrier for signal processing in VLC IoT networks. To overcome the challenge, we derived both the inner and outer bounds of the channel capacity region for uplink NOMA of VLC IoT networks.

2.1. Capacity Region with Discrete Inputs. As in the previous section, we assumed that the signal s_i is a discrete random variable with M_i real values $\{a_{i,m}\}_{1\leq m\leq M_i}$.

Specifically, the signal s_i satisfies

$$\Pr\left\{s_i = a_{i,m}\right\} = p_{i,m}, m = 1, \cdots, M_i, \tag{4a}$$

$$\mathbb{E}\{s_i\} = \sum_{m=1}^{M_i} p_{i,m} a_{i,m} = 0, \tag{4b}$$

$$\mathbb{E}\left\{s_i^2\right\} = \sum_{m=1}^{M_i} p_{i,m} a_{i,m}^2 = \varepsilon_i, \tag{4c}$$

$$\sum_{m=1}^{M_i} p_{i,m} = 1, -A_i \leq a_{i,m} \leq A_i, k = 1, \cdots, M_i, \tag{4d}$$

where $a_{i,m}$ denotes the mth point for signal s_i and $p_{i,m}$ denotes the corresponding probability.

2.1.1. Inner Bound with Discrete Inputs. Let R_i denote the capacity of user i, where $1 \leq i \leq N$, the capacity of R_i can be written as

$$\begin{aligned} R_i &= \max_{\{P(s_i)\}} I(y\,; s_i | s_1, \cdots, s_{i-1}), \\ &= \max_{\{P(s_i)\}} h(y|s_1, \cdots, s_{i-1}) - h(y|s_1, \cdots, s_i), \\ &= \max_{\{P(s_i)\}} h\left(\sum_{k=i}^{N} g_k \sqrt{p_k} s_k + z\right) - h\left(\sum_{j=i+1}^{N} g_j \sqrt{p_j} s_j + z\right), \\ &\geq \max_{\{P(s_i)\}} \frac{1}{2}\log_2 \sum_{k=i}^{N} 2^{2h(\widehat{y}_k)} - \frac{1}{2}\log_2 2\pi e\left(\sum_{j=i+1}^{N} g_j^2 p_j \varepsilon_j + \sigma^2\right), \end{aligned} \tag{5}$$

where $\widehat{y}_k = g_k\sqrt{p_k}s_k + \widehat{z}_k$, $\sum_{k=i}^K \widehat{z}_k = z$, due to the entropy power inequality (EPI) [21] and $h(Q) \leq 1/2 \log 2\pi e$ var (Q) for a random variable with variance, var (Q).

Based on (5), the discrete inner bound uplink NOMA of VLC can be obtained by maximizing the entropy $h(\widehat{y}_i)$, i.e.,

$$h(\widehat{y}_i) = -\int_{-\infty}^{\infty} f_{\widehat{Y}_i}(y) \log_2 f_{\widehat{Y}_i}(y) dy. \tag{6}$$

As the noise $\widehat{z}_{k,i}$ follows the Gaussian distribution with zero mean and σ^2/K variance, the probability density function (PDF) $f_Y(y)$ is given by

$$f_{\widehat{Y}_i}(y) = \frac{\sqrt{K}}{\sqrt{2\pi}\sigma} \sum_{m=1}^{M_i} p_{i,m} e^{-K(y - g_i\sqrt{p_i}a_{i,m})^2/2\sigma^2}. \tag{7}$$

Thus, the entropy $h(\widehat{y}_i)$ maximization problem is given by

$$\begin{aligned} \min_{M_i, \{a_{i,m}\}, \{p_{i,m}\}} \quad & \int_{-\infty}^{\infty} f_{\widehat{Y}_i}(y) \log_2 f_{\widehat{Y}_i}(y) dy \\ \text{s.t.} \quad & (4a), (4b), (4c), (4d). \end{aligned} \tag{8}$$

Problem (8) is a mixed discrete and nonconvex problem that is generally difficult to solve.

To handle Problem (8), we first defined some vectors as follows:

$$\begin{aligned} \mathbf{a}_i &\triangleq [a_{i,}1, \cdots, a_i, M_i]^T, \\ \mathbf{p}_i &\triangleq \left[p_{i,}1, \cdots, p_i, M_i\right]^T, \\ \mathbf{q}_i &\triangleq \frac{\sqrt{K}}{\sqrt{2\pi}\sigma}\left[e^{-K(y-g_i\sqrt{p_i}a_{i,1})^2/2\sigma^2}, \cdots, e^{-K(y-g_i\sqrt{p_i}a_i,M_i)^2/2\sigma^2}\right]^T. \end{aligned} \tag{9}$$

Based on the above mentioned definitions in (9), we reformulated Problem (8) as

$$\begin{aligned}\min_{M_i \mathbf{a}_i, \mathbf{p}_i} \int_{-\infty}^{\infty} & \mathbf{p}_i \mathbf{q}_i \log_2 \mathbf{p}_i \mathbf{q}_i \mathrm{d}y, \\ \text{s.t. } & \mathbf{p}_i^T \mathbf{a}_i = 0, \\ & \mathbf{p}_i^T (\mathbf{a}_i \odot \mathbf{a}_i) = \varepsilon_i, \\ & \mathbf{p}_i^T 1 M_i = 1, \\ & \mathbf{p}_i \geq 0,\end{aligned} \tag{10}$$

where $\odot$ denotes the Hadamard product. Note that given both M_i and $\mathbf{a}_i$, Problem (10), is convex with respect to $\mathbf{p}_i$, which can be solved efficiently using the available interior-point algorithms [32, 33].

Without the loss of generality, we assumed the space among the M_i points $\{a_{i,m}\}_{m=1}^{M_i}$ is equally placed in the range of $[-A_i, A_i]$, i.e.,

$$a_{i,m} = \frac{2A_i}{M_i - 1}(m_i - 1) - A_i. \tag{11}$$

Note that when M_i is larger than the optimal values M_i^*, redundant points exist in $\{a_{i,m}\}_{m=1}^{M_i}$. However, the effects of the redundant points can be eliminated by optimizing the PDF $\mathbf{p}_i$. Thus, for a sufficiently large M_i, the maximum entropy $h(\hat{y}_i)$ can be approximated by solving Problem (10) under condition (11). In summary, the proposed entropy $h(\hat{y}_i)$ approximation method is listed in Algorithm 1.

Let $h^*(\hat{y}_i)$ denote the entropy $h(\hat{y}_i)$ computed by Algorithm 1. Substituting $h^*(\hat{y}_i)$ to, we obtained the discrete inner bound of NOMA VLC as

$$R_i \geq \frac{1}{2}\log_2 \frac{\sum_{k=1}^{N} 2^{2h^*(\hat{y}_k)}}{2\pi e\left(\sum_{j=i+1}^{N} g_j^2 p_j \varepsilon_j + \sigma^2\right)}. \tag{12}$$

Let $\mathscr{R}_{\text{dis}}^{\text{inner}}$ denote the achievable rate region of NOMA VLC IoT networks bounded by (12), which is given by

$$\mathscr{R}_{\text{dis}}^{\text{inner}} \triangleq \left\{ \begin{array}{c} r_{1,\dots,}r_N | r_i \in \mathbb{R}, \\ r_i \geq \dfrac{1}{2}\log_2 \dfrac{\sum_{k=i}^{N} 2^{2h^*(\hat{y}k)}}{2\pi e\left(\sum_{j=i+1}^{N} g_j^2 p_j \sigma^2\right)}, \\ i = 1, \cdots, N. \end{array} \right\} \tag{13}$$

2.1.2. Outer Bound with Discrete Inputs. In this subsection, the outer bound of the channel capacity region of the NOMA VLC IoT network with discrete input is proposed. The upper bound of the achievable rate R_i is given by

$$R_i = \max_{\{P(s_i)\}} h\left(\sum_{k=i}^{N} g_k \sqrt{p_k} s_k + z\right) - h\left(\sum_{j=i+1}^{N} g_j \sqrt{p_j} s_j + z\right), \tag{14a}$$

$$\leq \frac{1}{2}\log_2 2\pi e \operatorname{var}\left(\sum_{k=i}^{N} g_k \sqrt{p_k} s_k + z\right) - \max_{\{f(s_i)\}} \frac{1}{2}\log_2 \sum_{j=i+1}^{N} 2^{2h(\hat{y}_i)}, \tag{14b}$$

$$= \frac{1}{2}\log_2 \frac{2\pi e\sigma^2 + 2\pi e\sum_{k=i}^{N} g_k^2 p_k \varepsilon_k}{\sum_{j=i+1}^{N} 2^{2h(\hat{y}_j)}}, \tag{14c}$$

where the inequality (14a) follows the EPI [21] and $h(x) \leq 1/2 \log 2\pi e \operatorname{var}(x)$ and $h^*(\hat{y}_i)$ is calculated by Algorithm $\mathscr{R}_{\text{dis}}^{\text{outer}}$ denotes the channel capacity region of NOMA VLC IoT networks bounded, which is given by

$$\mathscr{R}_{\text{dis}}^{\text{outer}} \triangleq \left\{ \begin{array}{c} r_{1,\dots,}r_N | r_i \in \mathbb{R}, \\ r_i \leq \dfrac{1}{2}\log_2 \dfrac{2\pi e\sigma^2 + 2\pi e\sum_{j=i}^{N} g_j^2 p_j \varepsilon_j}{\sum_{k=i+1}^{N} 2^{2h^*(\hat{y}_k)}}, \\ i = 1, \cdots, N. \end{array} \right\} \tag{15}$$

2.2. Capacity Region with Continuous Inputs. Although the discrete inner and outer bounds are obtained, they are not in closed-forms, which is the main obstacle in determining the capacity region. To this end, we assumed that the input signal s_i follows a continuous distribution and derived the ABG inner bound of NOMA VLC IoT networks in closed-form expressions.

2.2.1. ABG Inner Bound. Let $f(s_i)$ denote the pdf of s_i which satisfies the following peak optical power (Equation (16a)), average optical power (Equation (16b)), and electrical power constraints (Equation (16c)), i.e.,

$$\int_{-A_i}^{A_i} f(s_i) ds_i = 1, \tag{16a}$$

$$\int_{-A_i}^{A_i} s_i f(s_i) ds_i = 0, \tag{16b}$$

$$\int_{-A_i}^{A_i} s_i^2 f(s_i) ds_i = \varepsilon_i. \tag{16c}$$

Then, for $1 \leq i \leq N$, the lower bound of the achievable rate, R_i, is given by

$$R_i = \max_{\{f(s_i)\}} I(y; s_i | s_1, \cdots, s_{i-1}), \tag{17a}$$

$$= \max_{\{P(s_i)\}} h\left(\sum_{k=i}^{N} g_k \sqrt{p_k} s_k + z\right) - h\left(\sum_{j=i+1}^{N} g_j \sqrt{p_j} s_j + z\right), \tag{17b}$$

1 initialization: Set $n = 0$, $h_0 = 0$; set c_1 as the stopping parameter, choose $M_i \geq 2$;
2 let $n = n + 1$, and compute a_i according to (11);
3 compute the entropy $h_n = h(\hat{y}_i)$ by solving Problem (10);
4 if $|h_n - h_n - 1| \leq c_1$, stop, and output h_n; otherwise, $M_i = M_i + 1$, and go to step 2.

Algorithm 1. Entropy $h(\hat{y}_i)$ approximation method.

$$\begin{aligned} &\geq \max_{\{f(s_i)\}} \frac{1}{2} \log_2 \left(\sum_{k=i}^{N} 2^{2h(s_k)+\log_2 g_k^2 p_k} + 2^{2h(z)} \right) \\ &\quad - \frac{1}{2} \log_2 2\pi e \operatorname{var} \left(\sum_{j=i+1}^{N} g_j \sqrt{p_j} s_j + z \right), \end{aligned} \tag{17c}$$

$$= \frac{1}{2} \log_2 \frac{\sum_{k=i}^{N} p_k g_k^2 e^{1+2(\alpha_k+\gamma_k\varepsilon_k)} + 2\pi\sigma^2}{2\pi \sum_{j=i+1}^{N} p_j g_j^2 \varepsilon_j + 2\pi\sigma^2}, \tag{17d}$$

where the inequality (17c) is true due to the EPI [21] and $h(Q) \leq 1/2 \log 2\pi e \operatorname{var}(Q)$ for a random variable with variance, var (Q). The equality (17d) holds because the corresponding input distribution (termed ABG distribution) [34] maximizes the differential entropy and is given by

$$f_i(s_i) = \begin{cases} e^{-1-\alpha_i-\beta_i s_i - \gamma_i s_i^2}, & -A_i \leq s_i \leq A_i\,; \\ 0, & \text{otherwise}, \end{cases} \tag{18}$$

where the parameters α_i, β_i, and γ_i are the solutions of the following equations:

$$\begin{aligned} &T_i(A_i) - T_i(-A_i) = e^{1+\alpha_i}, \\ &\beta_i \left(e^{A_i(\beta_i - \gamma_i A_i)} - e^{1+\alpha_i} - e^{-A_i(\beta_i+\gamma_i A_i)} \right) = 0, \\ &e^{A_i(\beta_i-\gamma_i A_i)} \left((\beta_i - 2\gamma_i A_i) e^{-2A_i\beta_i} - \beta_i - 2\gamma_i A_i \right) + \left(\beta_i^2 + 2\gamma_i \right) e^{1+\alpha_i} \\ &\quad = 4\gamma_i^2 \varepsilon_i e^{1+\alpha i}, \end{aligned} \tag{19}$$

$$T_i(X) = \sqrt{\pi} \frac{e^{\beta_i^2/4\gamma_i} \operatorname{erf}\left(\beta_i + 2\gamma_i X / 2\sqrt{\gamma_i}\right)}{2\sqrt{\gamma_i}}. \tag{20}$$

For $k = N$, the upper bound R_k is given by

$$R_N = \frac{1}{2} \log_2 \left(1 + \frac{p_N g_N^2 e^{1+2(\alpha_N + \gamma N \varepsilon N)}}{2\pi\sigma^2} \right) \tag{21}$$

Let $\mathscr{R}_{\text{con}}^{\text{inner}}$ denote the achievable rate region of NOMA VLC, which is given by

$$\mathscr{R}_{\text{con}}^{\text{inner}} \triangleq \left\{ \begin{array}{c} r_1, \cdots, r_K | r_i \in \mathbb{R}, \\ r_i \geq \dfrac{1}{2} \log_2 \dfrac{\sum_{k=i}^{N} p_k g_k^2 e^{1+2(\alpha_k+\gamma_k\varepsilon_k)} + 2\pi\sigma^2}{2\pi \sum_{j=i+1}^{N} p_j g_j^2 \varepsilon_j + 2\pi\sigma^2}, \\ i = 1, \cdots, K. \end{array} \right\} \tag{22}$$

2.2.2. ABG Outer Bound. Finally, we developed the ABG outer bound of uplink NOMA of VLC IoT networks in closed-form expressions for the continuous input. The upper bound of the maximum achievable rate, R_i, is given by

$$R_i = \max_{\{f(s_i)\}} h\left(\sum_{k=i}^{N} g_k \sqrt{p_k} s_k + z \right) - h\left(\sum_{j=i+1}^{N} g_j \sqrt{p_j} s_j + z \right), \tag{23a}$$

$$\begin{aligned} &\leq \frac{1}{2} \log_2 2\pi e \operatorname{var} \left(\sum_{k=i}^{N} g_k \sqrt{p_k} s_k + z \right) \\ &\quad - \max_{\{f(s_i)\}} \frac{1}{2} \log_2 \left(\sum_{j=i+1}^{N} 2^{2h(s_j)+\log_2 g_j^2 p_j} + 2^{2h(z)} \right), \end{aligned} \tag{23b}$$

$$= \frac{1}{2} \log_2 \frac{2\pi\sigma^2 + 2\pi \sum_{k=i}^{N} g_k^2 p_k \varepsilon_k}{\sum_{j=i+1}^{N} p_j g_j^2 e^{1+2(\alpha_j+\gamma_j\varepsilon_j)} + 2\pi\sigma^2}, \tag{23c}$$

where the inequality (23b) follows the EPI [21] and $h(Q) \leq 1/2 \log 2\pi e \operatorname{var}(x)$ and the equality (23c) holds because s_i follows the ABG distribution [34].

Let $\mathscr{R}_{\text{con}}^{\text{outer}}$ denote the channel capacity region of NOMA VLC IoT networks bounded by (23c), which is given by

$$\mathscr{R}_{\text{con}}^{\text{outer}} \triangleq \left\{ \begin{array}{c} r_1, \cdots, r_N | r_i \in \mathbb{R}, \\ r_i \leq \dfrac{1}{2} \log_2 \dfrac{2\pi\sigma^2 + 2\pi \sum_{j=i}^{N} g_j^2 p_j \varepsilon_j}{\sum_{k=i+1}^{N} p_k g_k^2 e^{1+2(\alpha_k+\gamma_k\varepsilon_k)}{}_j + 2\pi\sigma^2}, \\ i = 1, \cdots, K \end{array} \right\}. \tag{24}$$

3. Optimal Beamforming Design for Uplink NOMA of VLC IOT Networks

In this section, we further considered a single-input, multiple-output (SIMO) uplink NOMA for a VLC IoT network as illustrated in Figure 2, which includes N single

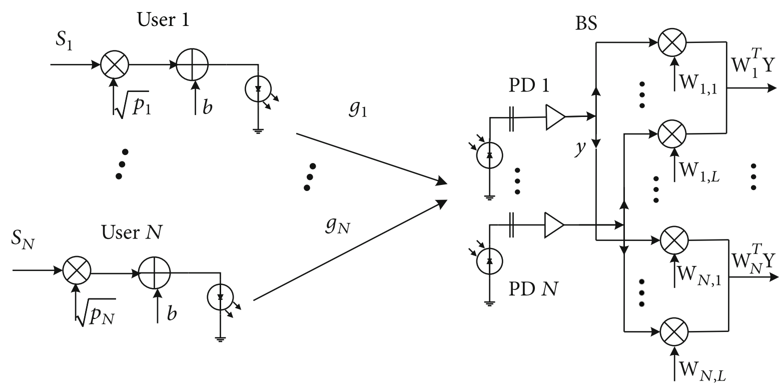

FIGURE 2: Schematic of SIMO NOMA of a VLC IoT network.

LED users (IoT devices) and a L PDs BS. Let s_i denote the transmitted message from user i, where the definition of s_i is similar to that in the previous SISO scenario. Thus, the received signal at BS can be expressed as

$$\mathbf{y} = \sum_{k=1}^{N} \mathbf{g}_k \sqrt{p_k} s_k + \mathbf{z}, \tag{25}$$

where $\mathbf{g}_i \in \mathbb{R}^{L\times 1}$ denotes the channel vector between user i and BS, $p_i \varepsilon_i \geq 0$ is the transmitted power of user i, and $\mathbf{z} \sim \mathcal{N}(\mathbf{0}, \sigma^2 \mathbf{I})$ represents the additive white Gaussian noise vector.

For message s_i, the BS invokes a linear receive beamformer $\mathbf{w}_i \in \mathbb{R}^L$ to the received signals $\mathbf{y}$ as follows:

$$\widehat{y}_i = \mathbf{w}_i^T \mathbf{y} = \sum_{k=1}^{N} \mathbf{w}_i^T \mathbf{g}_k \sqrt{p_k} s_k + \mathbf{w}_i^T \mathbf{z}, i = 1, \cdots, N. \tag{26}$$

Without the loss of generality, we assumed that the terms $\{\|\mathbf{g}_i^T \sqrt{p_i \varepsilon_i}\|\}_{i=1}^N$ satisfy a descending order, i.e., $\|\mathbf{g}_1^T \sqrt{p_1 \varepsilon_1}\| \geq \|\mathbf{g}_2^T \sqrt{p_2 \varepsilon_2}\| \geq \cdots \geq \|\mathbf{g}_N^T \sqrt{p_N \varepsilon_N}\|$. Then, the BS adopts the SIC technique to decode the received signals in a descending order [35], i.e., from s_1 to s_N. Specifically, let R_i denote the achievable rate of decoding message s_i, $1 \leq i \leq N$.

When $1 \leq i < N$, R_i is given by

$$R_i = \max_{\{f(s_i)\}} I(\widehat{y}\,; s_i | s_1, \cdots, s_{i-1}), \tag{27a}$$

$$= \max_{\{f(s_i)\}} h(\widehat{y} | s_1, \cdots, s_{i-1}) - h(\widehat{y} | s_1, \cdots, s_i), \tag{27b}$$

$$= \max_{\{f(s_i)\}} h\left(\sum_{j=i}^{N} \mathbf{w}_i^T \mathbf{g}_j \sqrt{p_j} s_j + \mathbf{w}_i^T \mathbf{z}\right) - h\left(\sum_{m=i+1}^{N} \mathbf{w}_k^T \mathbf{g}_m \sqrt{p_m} s_m + \mathbf{w}_i^T \mathbf{z}\right), \tag{27c}$$

$$\geq \max_{\{f(s_i)\}} \frac{1}{2} \log_2 \left(\sum_{j=i}^{N} 2^{2h(s_j)} + \log_2 \left|\mathbf{w}_i^T \mathbf{g}_j\right|^2 p_j + 2^{2h\left(\mathbf{w}_i^T \mathbf{z}\right)} \right) - \frac{1}{2} \log_2 2\pi e \operatorname{var} \left(\sum_{m=i+1}^{N} \left|\mathbf{w}_i^T \mathbf{g}_m\right|^2 + p_m s_m + \|\mathbf{w}_i\|^2 \sigma^2 \right), \tag{27d}$$

$$= \frac{1}{2} \log_2 \frac{\sum_{j=i}^{N} \left|\mathbf{w}_i^T \mathbf{g}_j\right|^2 p_j e^{1+2\left(\alpha_j + \gamma_j \varepsilon_j\right)} + 2\pi \|\mathbf{w}_i\|^2 \sigma^2}{2\pi \sum_{m=i+1}^{N} \left|\mathbf{w}_i^T \mathbf{g}_m\right|^2 p_m \varepsilon_m + 2\pi \|\mathbf{w}_i\|^2 \sigma^2}, \tag{27e}$$

where the inequality (27d) holds due to the EPI [21] and $h(Q) \leq (1/2) \log 2\pi e \operatorname{var}(Q)$ for a random variable with variance, var (Q). The equality (27e) holds because the corresponding input distribution (termed ABG distribution) [34] maximizes the differential entropy. For $k = N$, R_N is given by

$$R_N = \frac{1}{2} \log_2 \left(1 + \frac{\left|\mathbf{w}_N^T \mathbf{g}_N\right|^2 p_N e^{1+2(\alpha_N + \gamma_N \varepsilon_N)}}{2\pi \sigma^2} \right). \tag{28}$$

Therefore, for $1 \leq i \leq N$, the expression of the lower bound R_i can be expressed as

$$R_i = \frac{1}{2} \log_2 \frac{\sum_{j=i}^{N} \left|\mathbf{w}_i^T \mathbf{g}_j\right|^2 p_j e^{1+2\left(\alpha_j + \gamma_j \varepsilon_j\right)} + 2\pi \|\mathbf{w}_i\|^2 \sigma^2}{2\pi \Gamma_i \sum_{m=i+1}^{N} \left|\mathbf{w}_i^T \mathbf{g}_m\right|^2 p_m \varepsilon_m + 2\pi \|\mathbf{w}_i\|^2 \sigma^2}, \tag{29}$$

where Γ_i is an indicator function as follows:

$$\Gamma_i \triangleq \begin{cases} 1, & \forall_i \neq N, \\ 0, & i = N. \end{cases} \tag{30}$$

Based on the explicit achievable rate expression in (29), we investigated the optimal receiver beamformers' design to maximize the minimum achievable rates which satisfies the

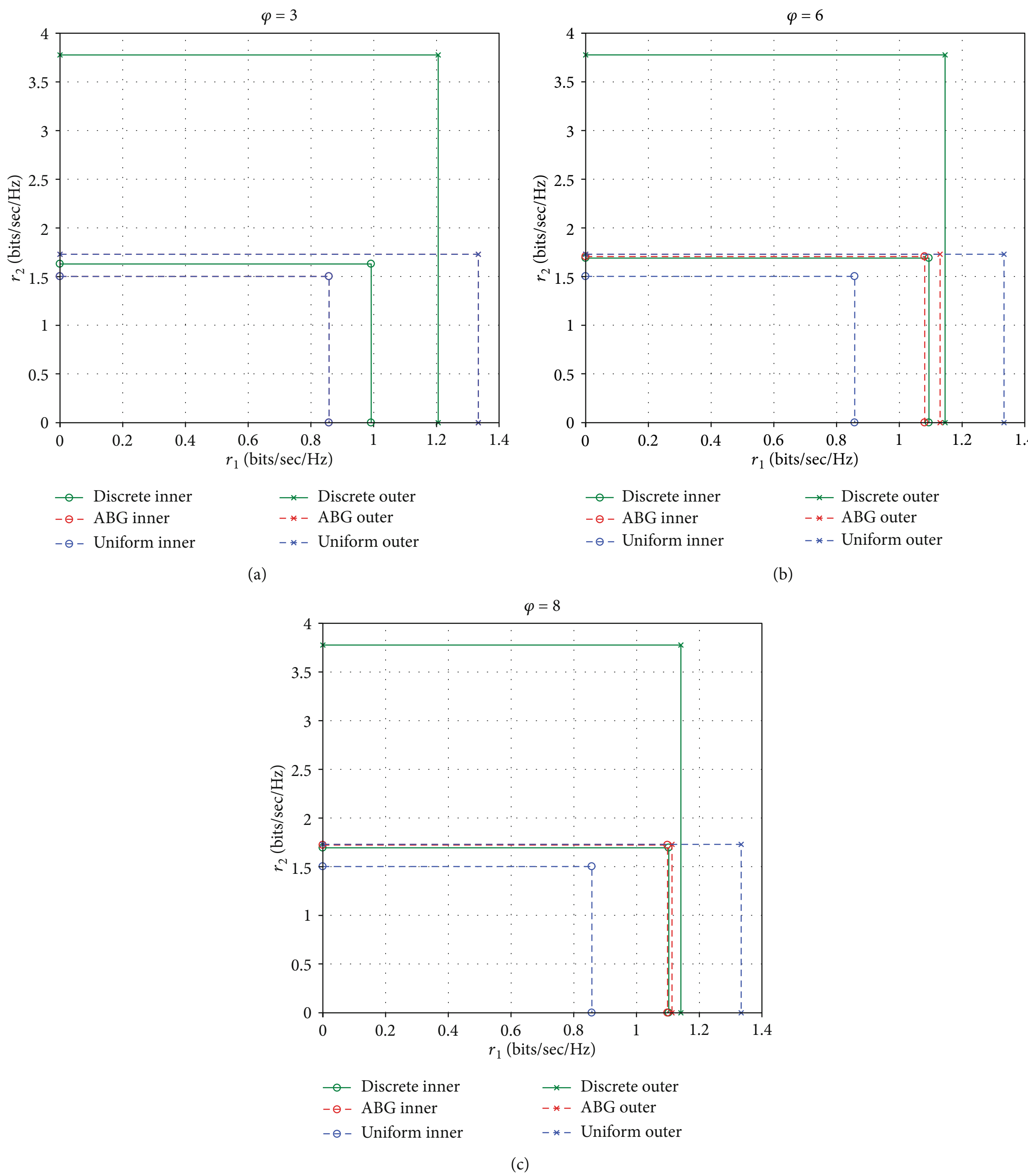

Figure 3: Outer and inner bounds of the capacity region for MAC NOMA in VLC IoT networks with (a) $\varphi = 3$, (b) $\varphi = 6$, and (c) $\varphi = 8$, respectively.

power constraints as follows:

$$\max_{\mathbf{w}_i} \frac{1}{2}\log_2 \frac{\sum_{j=i}^{N}\left|\mathbf{w}_i^T\mathbf{g}_j\right|^2 p_j e^{1+2\left(\alpha_j+\gamma_j\varepsilon_j\right)} + 2\pi\|\mathbf{w}_i\|^2\sigma^2}{2\pi\Gamma_i\sum_{m=i+1}^{N}\left|\mathbf{w}_i^T\mathbf{g}_m\right|^2 p_m\varepsilon_m + 2\pi\|\mathbf{w}_i\|^2\sigma^2} \quad (31)$$
$$\text{s.t.} \|\mathbf{w}_i\|^2 \le 1, 1 \le i \le N.$$

Note that Problem (31) is nonconvex which is hard to solve. To deal with this difficulty, we first define some variables as follows:

$$\begin{aligned} \widehat{p}_i &= \sqrt{p_i e^{1+2(\alpha_i+\gamma_i\varepsilon_i)}},\\ \mathbf{G}_i &\triangleq [0, \cdots, \widehat{p}_i\mathbf{g}_i, \cdots, \widehat{p}_N\mathbf{g}_N],\\ \bar{\mathbf{G}}_i &\triangleq 2\pi[\mathbf{0}, \cdots, \Gamma_i\sqrt{p_{i+1}\varepsilon_{i+1}}\mathbf{g}_i, \cdots, \Gamma_i\sqrt{p_N\varepsilon_N}\mathbf{g}_N],\\ c &\triangleq 2\pi\sigma^2. \end{aligned} \quad (32)$$

With the introduced variables in (32), we can equivalently rewrite Problem (31) to a concise form as follows:

$$\max_{\mathbf{w}_i} \frac{1}{2}\log_2\left(\frac{\mathbf{w}_i^T\mathbf{G}_i\mathbf{G}_i^T\mathbf{w}_i + c\mathbf{w}_i^T\mathbf{w}_i}{\mathbf{w}_i^T\bar{\mathbf{G}}_i\bar{\mathbf{G}}_i^T\mathbf{w}_i + c\mathbf{w}_i^T\mathbf{w}_i}\right), \quad (33)$$
$$\text{s.t.} \|\mathbf{w}_i\|^2 \le 1, 1 \le i \le N,$$

which is a quadratically constrained quadratic problem (QCQP). As the logarithmic function is monotonically increasing, Problem (33) can be further reformulated as follows:

$$\max_{\mathbf{w}_i} \frac{\mathbf{w}_i^T\left(\mathbf{G}_i\mathbf{G}_i^T + c\mathbf{I}\right)\mathbf{w}_i}{\mathbf{w}_i^T\left(\mathbf{G}_i\mathbf{G}_i^T + c\mathbf{I}\right)\mathbf{w}_i} \quad (34)$$
$$\text{s.t.} \|\mathbf{w}_i\|^2 \le 1, 1 \le i \le N.$$

Let $\lambda_{i,\max}$ denote the largest generalized eigenvalue of matrix $\mathbf{A}_i$ and matrix $\mathbf{B}_i$, where $\mathbf{A}_i \triangleq \mathbf{G}_i\mathbf{G}_i^T + c\mathbf{I}$ and $\mathbf{B}_i \triangleq \bar{\mathbf{G}}_i\bar{\mathbf{G}}_i^T + c\mathbf{I}$.

Furthermore, let $\mathbf{w}_{i,\max}$ denote the generalized eigenvector corresponding to the largest eigenvalue $\lambda_{i,\max}$, which satisfies $\mathbf{A}_\mathbf{i}\mathbf{w}_{i,\max} = \lambda_{i,\max}\mathbf{B}_\mathbf{i}\mathbf{w}_{i,\max}$. Thus, for the NOMA VLC uplink, the optimal beamformer $\mathbf{w}_i$ of Problem (34) is given by

$$\mathbf{w}_i^{\text{opt}} = \frac{\mathbf{w}_{i,\max}}{\left\|\mathbf{w}_{i,\max}\right\|}, \quad (35)$$

and the maximum achievable rate of message s_i is $\log_2\lambda_{i,\max}$.

4. Numerical Results

In this section, the performance of the capacity region and the optimal beamforming design for uplink NOMA in VLC IoT networks are evaluated using numerical results.

In the following, we present the performance of the discrete inner and outer bounds and the ABG inner and outer bounds of the capacity region for the MAC NOMA in VLC IoT networks. Assume that $g_1 = 1$, $g_2 = 1/2$, $A \triangleq A_1 = A_2$, and $\varepsilon \triangleq \varepsilon_1 = \varepsilon_2$. Let $\varphi \triangleq A^2/\varepsilon$ denote the amplitude-to-variance ratio, and define SNR as $\triangleq \varepsilon/\sigma^2$. Moreover, both the uniform inner and outer bounds of the capacity region of MAC NOMA of VLC IoT networks are also presented

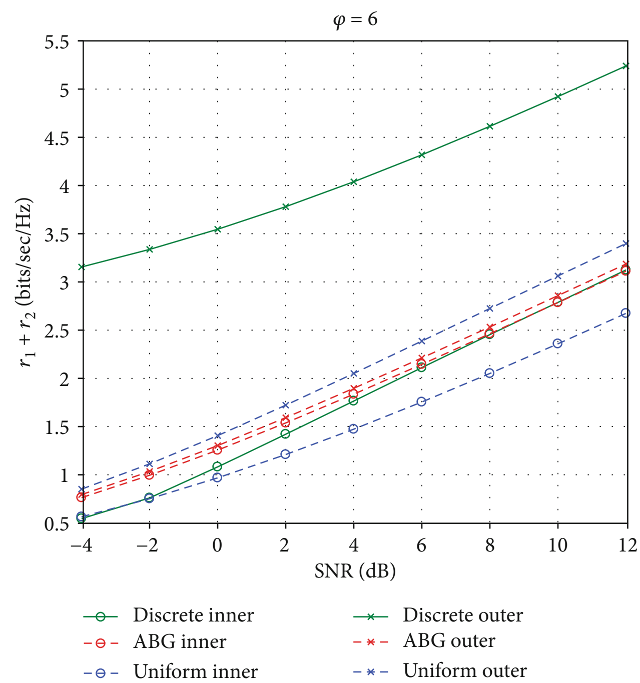

Figure 4: Sum rates $r_1 + r_2$ (bits/sec/Hz) of the discrete inner and outer bounds, ABG inner and outer bounds, and uniform inner and outer bounds versus SNR(dB) with $\varphi = 6$.

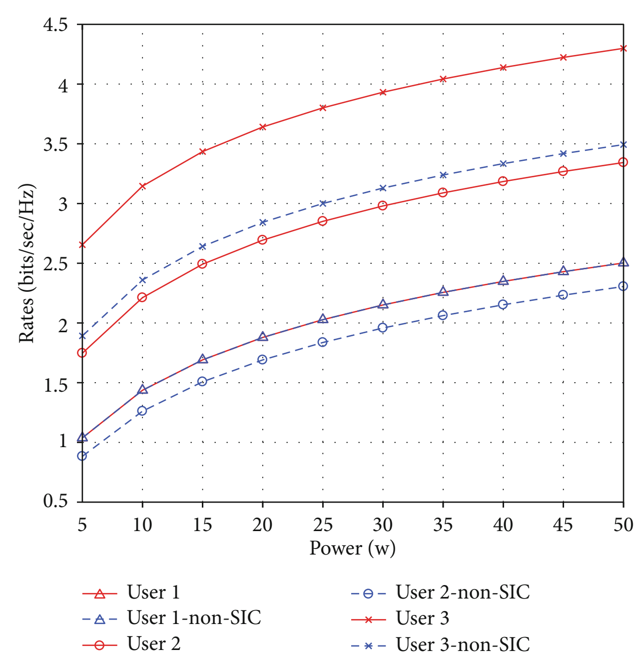

Figure 5: Maximum rates of users versus transmit power.

for comparison, where the input signals follow a uniform distribution [36–38].

Figures 3(a)–3(c) show the inner and outer bounds for the channel capacity region of uplink NOMA in VLC IoT networks with $\mathrm{SNR} = 10\,\mathrm{dB}$, $\varphi = 3$, 6, and 8, respectively. Figure 3(a) shows that the ABG inner bound is identical to the uniform inner bound. A similar case is observed for the outer bound; this is because the ABG has a uniform distribution for $\varphi = 3$. Moreover, the inner bound with discrete inputs is larger than the ABG inner bound, while the outer bound with discrete inputs cannot dominate the ABG outer bound. Figures 3(b) and 3(c) show that the inner bound with discrete inputs is the highest among the three types of inner bounds, while the ABG outer bound is the lowest among the three types of outer bounds for $\varphi = 6$ and 8. Comparing Figures 3(a)–3(c), it can be seen that as the value of φ increases, the gap between the inner bound with discrete input and the ABG inner bound decreases, and the gap between the ABG inner bound and the ABG outer bound also decreases.

Figure 4 compares the sum rates $r_1 + r_2$ (bits/sec/Hz) of the discrete inner and outer bounds, the ABG inner and outer bounds, and the uniform and inner bounds against SNR(dB) with $\phi = 6$. As shown in Figure 4, the sum rate of each bound increases as the SNR gets larger, and the ABG inner bound is higher than those with the discrete inputs and the uniform inner bound, while the ABG outer bound is lower than the one with discrete inputs and the uniform outer bound. Additionally, we can observe that the gap between the proposed ABG inner bound and ABG outer bound increases as the SNR increases.

Figure 5 shows the achievable rates of three users with respect to the transmit power. We can see that the rate of each user increases as the rate of the transmit power increases. Furthermore, the rate for each user of the proposed method is larger than that of the users of the non-SIC methods.

5. Conclusions

In this paper, we investigated the NOMA transmission for VLC IoT networks. Specifically, the channel capacity region of the practical NOMA VLC IoT networks was established with discrete and continuous inputs, respectively. To the best of our knowledge, the proposed inner and outer bounds are the first theoretical bounds of the channel capacity region for uplink NOMA of VLC IoT networks. Furthermore, we developed the optimal receiver NOMA beamforming design for VLC IoT networks and showed that the optimal beamformers are the generalized eigenvectors corresponding to the largest generalized eigenvalues.

Data Availability

The data of the numerical results can be obtained by emailing the author (mashuai001@cumt.edu.cn).

Conflicts of Interest

The authors declare that they have no conflicts of interest.

Acknowledgments

This work was supported by the National Natural Science Foundation of China (nos. 61701501 and 61771474), by the Natural Science Foundation of Jiangsu Province (no. BK20170287), by the Key Laboratory of Ocean Observation-Imaging Testbed of Zhejiang Province, by the Young Talents of Xuzhou Science and Technology Plan Project under Grant KC19051, and by the Key Laboratory of Cognitive Radio and Information Processing, Ministry of Education (Guilin University of Electronic Technology) under Grant CRKL180204.

References

[1] T. Komine and M. Nakagawa, "Fundamental analysis for visible-light communication system using LED lights," *IEEE Transactions on Consumer Electronics*, vol. 50, no. 1, pp. 100–107, 2004.

[2] H. Elgala, R. Mesleh, and H. Haas, "Indoor optical wireless communication: potential and state-of-the-art," *IEEE Communications Magazine*, vol. 49, no. 9, pp. 56–62, 2011.

[3] S. Arnon, J. Barry, G. Karagiannidis, R. Schober, and M. Uysal, *Advanced Optical Wireless Communication Systems*, Cambridge Univ, Cambridge, U.K., 1st edition, 2012.

[4] A. Jovicic, J. Li, and T. Richardson, "Visible light communication: opportunities, challenges and the path to market," *IEEE Communications Magazine*, vol. 51, no. 12, pp. 26–32, 2013.

[5] P. H. Pathak, X. Feng, P. Hu, and P. Mohapatra, "Visible light communication, networking, and sensing: a survey, potential and challenges," *IEEE Communications Surveys & Tutorials*, vol. 17, no. 4, pp. 2047–2077, 2015.

[6] D. Karunatilaka, F. Zafar, V. Kalavally, and R. Parthiban, "LED based indoor visible light communications: state of the art," *IEEE Communications Surveys & Tutorials*, vol. 17, no. 3, pp. 1649–1678, 2015.

[7] J. Luo, L. Fan, and H. Li, "Indoor positioning systems based on visible light communication: state of the art," *IEEE Communications Surveys & Tutorials*, vol. 19, no. 4, pp. 2871–2893, 2017.

[8] L. Dai, B. Wang, Y. Yuan, S. Han, Chih-lin I, and Z. Wang, "Non-orthogonal multiple access for 5G: solutions, challenges, opportunities, and future research trends," *IEEE Communications Magazine*, vol. 53, no. 9, pp. 74–81, 2015.

[9] X. Li, J. Li, Y. Liu, Z. Ding, and A. Nallanathan, "Residual transceiver hardware impairments on cooperative NOMA networks," *IEEE Transactions on Wireless Communications*, vol. 19, no. 1, pp. 680–695, 2019.

[10] X. Li, M. Liu, C. Deng, P. T. Mathiopoulos, Z. Ding, and Y. Liu, "Full-duplex cooperative noma relaying systems with i/q imbalance and imperfect sic," *IEEE Wireless Communications Letters*, vol. 9, no. 1, pp. 17–20, 2019.

[11] Z. Ding, Y. Liu, J. Choi et al., "Application of non-orthogonal multiple access in LTE and 5G networks," *IEEE Communications Magazine*, vol. 55, no. 2, pp. 185–191, 2017.

[12] W. Hao, Z. Chu, F. Zhou, S. Yang, G. Sun, and K. Wong, "Green communication for NOMA-based CRAN," *IEEE Internet of Things Journal*, vol. 6, no. 1, pp. 666–678, 2019.

[13] X. Li, J. Li, and L. Li, "Performance analysis of impaired swipt noma relaying networks over imperfect weibull channels," *IEEE Systems Journal*, vol. 14, no. 1, pp. 669–672, 2020.

[14] H. Tabassum, E. Hossain, and J. Hossain, "Modeling and analysis of uplink non-orthogonal multiple access (NOMA) in large-scale cellular networks using poisson cluster processes," *IEEE Transactions on Communications*, vol. 65, no. 8, pp. 1–3570, 2017.

[15] M. A. Sedaghat and R. R. Mller, "On user pairing in uplink NOMA," *IEEE Transactions on Wireless Communications*, vol. 17, no. 5, pp. 3474–3486, 2018.

[16] R. Ruby, S. Zhong, H. Yang, and K. Wu, "Enhanced uplink resource allocation in non-orthogonal multiple access systems," *IEEE Transactions on Wireless Communications*, vol. 17, no. 3, pp. 1432–1444, 2018.

[17] N. Zhang, T. Ding, and G. Kang, "Interference balance power control for uplink non-orthogonal multiple access," *IEEE Communications Letters*, vol. 23, no. 3, pp. 470–473, 2019.

[18] Z. Ding, R. Schober, and H. V. Poor, "A general MIMO framework for NOMA downlink and uplink transmission based on signal alignment," *IEEE Transactions on Wireless Communications*, vol. 15, no. 6, pp. 4438–4454, 2016.

[19] Z. Zhang, H. Sun, and R. Q. Hu, "Downlink and uplink non-orthogonal multiple access in a dense wireless network," *IEEE Journal on Selected Areas in Communications*, vol. 35, no. 12, pp. 2771–2784, 2017.

[20] X. Guan, Q. Yang, and C. Chan, "Joint detection of visible light communication signals under non-orthogonal multiple access," *IEEE Photonics Technology Letters*, vol. 29, no. 4, pp. 377–380, 2017.

[21] T. M. Cover and J. A. Thomas, *Elements of information theory*, Wiley, New York, 2nd edition, 2006.

[22] J. G. Smith, "The information capacity of amplitude- and variance-constrained sclar gaussian channels," *Information and Control*, vol. 18, no. 3, pp. 203–219, 1971.

[23] T. Fath and H. Haas, "Performance comparison of MIMO techniques for optical wireless communications in indoor environments," *IEEE Transactions on Communications*, vol. 61, no. 2, pp. 733–742, 2013.

[24] T. Q. Wang, Y. A. Sekercioglu, and J. Armstrong, "Analysis of an optical wireless receiver using a hemispherical lens with application in MIMO visible light communications," *Journal of Lightwave Technology*, vol. 31, no. 11, pp. 1744–1754, 2013.

[25] J. Kahn and J. Barry, "Wireless infrared communications," *Proceedings of the IEEE*, vol. 85, no. 2, pp. 265–298, 1997.

[26] S. M. Moser, "Capacity results of an optical intensity channel with input-dependent Gaussian noise," *IEEE Transactions on Information Theory*, vol. 58, no. 1, pp. 207–223, 2012.

[27] Q. Gao, C. Gong, and Z. Xu, "Joint transceiver and offset design for visible light communications with input-dependent shot noise," *IEEE Transactions on Wireless Communications*, vol. 16, no. 5, pp. 2736–2747, 2017.

[28] C. Gong, A. Tajer, and X. Wang, "Interference channel with constrained partial group decoding," *IEEE Transactions on Communications*, vol. 59, no. 11, pp. 3059–3071, 2011.

[29] X. Zhang, Q. Gao, C. Gong, and Z. Xu, "User grouping and power allocation for NOMA visible light communication multi-cell networks," *IEEE Communications Letters*, vol. 21, no. 4, pp. 777–780, 2017.

[30] Z. Yang, W. Xu, and Y. Li, "Fair non-orthogonal multiple access for visible light communication downlinks," *IEEE Wireless Communications Letters*, vol. 6, no. 1, pp. 66–69, 2017.

[31] Z. Ding, L. Dai, and H. V. Poor, "MIMO-NOMA design for small packet transmission in the Internet of Things," *IEEE Access*, vol. 4, pp. 1393–1405, 2016.

[32] J. F. Sturm, "Using SeDuMi 1.02, a Matlab toolbox for optimization over symmetric cones," *Optimization Methods and Software*, vol. 11, no. 1-4, pp. 625–653, 1999.

[33] M. Grant and S. Boyd, "CVX: Matlab software for disciplined convex programming," June 2009, http://stanford.edu/boyd/cvx.

[34] S. Ma, R. Yang, H. Li, Z.-L. Dong, H. Gu, and S. Li, "Achievable rate with closed-form for SISO channel and broadcast channel in visible light communication networks," *Journal of Lightwave Technology*, vol. 35, no. 14, pp. 2778–2787, 2017.

[35] M. Mollanoori and M. Ghaderi, "Uplink scheduling in wireless networks with successive interference cancellation," *IEEE Transactions on Mobile Computing*, vol. 13, no. 5, pp. 1132–1144, 2014.

[36] T. V. Pham and A. T. Pham, "Max-Min fairness and sum-rate maximization of MU-VLC local networks," in *2015 IEEE Globecom Workshops (GC Wkshps)*, pp. 1–6, San Diego, CA, USA, December 2015.

[37] T. V. Pham, H. L. Minh, and A. T. Pham, "Multi-cell VLC: multiuser downlink capacity with coordinated precoding," in *2017 IEEE International Conference on Communications Workshops (ICC Workshops)*, Paris, France, 2017.

[38] H. Shen, Y. Deng, W. Xu, and C. Zhao, "Rate-maximized zero-forcing beamforming for VLC multiuser MISO downlinks," *IEEE Photonics Journal*, vol. 8, no. 1, pp. 1–13, 2016.